

## Porohyperelastic anatomical models for hydrocephalus and idiopathic intracranial hypertension

Hakseung Kim, MEng,<sup>1</sup> Byoung-Kyong Min, PhD,<sup>1</sup> Dae-Hyeon Park, MEng,<sup>1</sup> Stanley Hawi, BEng,<sup>1</sup> Byung-Jo Kim, MD, PhD,<sup>2</sup> Zofia Czosnyka, PhD,<sup>3</sup> Marek Czosnyka, PhD,<sup>3</sup> Michael P. F. Sutcliffe, PhD,<sup>4</sup> and Dong-Joo Kim, PhD<sup>1</sup>

<sup>1</sup>Department of Brain and Cognitive Engineering, Korea University; <sup>2</sup>Department of Neurology, Korea University College of Medicine, Seoul, South Korea; <sup>3</sup>Department of Neurosurgery, Addenbrooke's Hospital, University of Cambridge; and <sup>4</sup>Department of Engineering, University of Cambridge, United Kingdom

**OBJECT** Brain deformation can be seen in hydrocephalus and idiopathic intracranial hypertension (IIH) via medical images. The phenomenology of local effects, brain shift, and raised intracranial pressure and herniation are textbook concepts. However, there are still uncertainties regarding the specific processes that occur when brain tissue is subject to the mechanical stress of different temporal and spatial profiles of the 2 neurological disorders. Moreover, recent studies suggest that IIH and hydrocephalus may be diseases with opposite pathogenesis. Nevertheless, the similarities and differences between the 2 subjects have not been thoroughly investigated.

**METHODS** An anatomical porohyperelastic finite element model was used to assess the brain tissue responses associated with hydrocephalus and IIH. The same set of boundary conditions, with the exception of brain loading for development of the transmante pressure gradient, was applied for the 2 models. The distribution of stress and strain during tissue distortion is described by the mechanical parameters.

**RESULTS** The results of both the hydrocephalus and IIH models correlated with pathological characteristics. For the hydrocephalus model, periventricular edema was associated with the presence of positive volumetric strain and void ratio in the lateral ventricle horns. By contrast, the IIH model revealed edema across the cerebral mantle, including the centrum semiovale, with a positive void ratio and volumetric strain.

**CONCLUSIONS** The model simulates all the clinical features in correlation with the MR images obtained in patients with hydrocephalus and IIH, thus providing support for the role of the transmante pressure gradient and capillary CSF absorption in CSF-related brain deformation. The finite element methods can be used for a better understanding of the pathophysiological mechanisms of neurological disorders associated with parenchymal volumetric fluctuation.

<http://thejns.org/doi/abs/10.3171/2014.12.JNS14516>

**KEY WORDS** biomechanics; bi-phase; finite element model; hydrocephalus; idiopathic intracranial hypertension; cerebrospinal fluid

**D**ISTURBANCES in CSF dynamics are known to contribute to the distortion of the brain parenchyma.<sup>48,66</sup> The most well-known form of brain deformation associated with CSF disturbance is found in patients with hydrocephalus. Within hydrocephalus, obstruction in CSF circulation leads to distortion of the brain, which in turn produces a series of clinical symptoms including headache, nausea, vomiting, and cognitive deterioration.<sup>10</sup>

Similar concerns regarding brain deformation occur in idiopathic intracranial hypertension (IIH), which is a neurological disease characterized by high intracranial pressure without apparent cause.<sup>6</sup> The symptoms of IIH also include headaches, but patients do not display any other typical signs of hydrocephalus.<sup>1</sup> Although the pathophysiological mechanism of IIH is largely unknown, the impaired capacity for CSF absorption is considered to be an

**ABBREVIATIONS** FE = finite element; FEM = FE model; IIH = idiopathic intracranial hypertension.

**SUBMITTED** March 7, 2014. **ACCEPTED** December 15, 2014.

**INCLUDE WHEN CITING** Published online February 6, 2015; DOI: 10.3171/2014.12.JNS14516.

**DISCLOSURE** Dr. M. Czosnyka is a consultant for J&J (Codman), and has received payment for lectures from Integra Lifescience. This research was supported by the Basic Science Research Program through the National Research Foundation of Korea (NRFK) funded by the Ministry of Science, ICT, & Future Planning (2013R1A1A1004827); and the International Research & Development Program of the NRFK funded by the Ministry of Education, Science, and Technology of Korea (Grant No. 2014K1A3A1A21001366).

important feature.<sup>37</sup> Some authors have suggested that the impaired capacity for CSF absorption in IIH may be due to resistance generated by raised venous pressure from venous outflow obstruction; however, the circumstances leading to this impairment are not yet clear.<sup>15</sup>

Several studies suggest that there may be a common physiological mechanism in IIH and hydrocephalus, but that it manifests as varying pathological phenomena.<sup>3,5,28</sup> Winston and Breeze hypothesized that the hydraulic regulation of parenchymal volume can be explained by the pressure differences of certain entities, such as capillary pressure, ventricular fluid pressure, and interstitial fluid pressure.<sup>65</sup> This possibility is a subject that requires further exploration. However, clinical observations or controlled trials regarding the subject would be difficult to conduct, not to mention the practical concerns involved.

Over the past 3 decades, significant research<sup>44,48,59</sup> has been conducted to examine the biomechanics involved in the reduction of the volume of the parenchyma, or deformation of the brain tissue.<sup>59</sup> In particular, finite element models (FEMs) have been developed to investigate the biomechanical behavior of hydrocephalus.<sup>55</sup> In FE analysis, the structure is divided into numerous small elements ("meshed"), thereby enabling numerical approximation of structural stress and deformation.<sup>69</sup> Since Nagashima et al.<sup>44</sup> first attempted to simulate the biomechanical features of the hydrocephalic brain, FE analysis of the hydrocephalic brain has been considered to be a valid approach.<sup>10,11,16,35,44,48,59,63,64,66</sup>

This work aims to investigate the idea of the active role of the pressure gradient in brain deformation<sup>36,48,65</sup> associated with IIH and hydrocephalus via an FEM of the brain that is capable of simulating both disorders. The FEM would simulate characteristic features of the 2 disorders such as brain deformation, enlarged or small ventricles, periventricular lucency, and tissue edema by manipulating the transmante pressure gradient level. In effect, the results of the present study will serve as indirect evidence for the hypothesized relationship between IIH and hydrocephalus.

## Methods

The FE method (Abaqus/Standard, Dassault Systèmes) was used because it allows for the modeling of complex domains and possesses the appropriate material properties, load histories, and boundary conditions.<sup>67</sup> The brain geometry was taken from a set of T2-weighted axial MR images of a human brain, and was obtained from the Wolfson Brain Imaging Centre, Addenbrooke's Hospital (University of Cambridge). To minimize the number of clinical factors related to hydrocephalus and IIH, the image was selected from among those of young, healthy adults (age 30 years) who had no radiological signs of neurological disorder. Given the symmetry of the brain in the section, only half of the slice was used.

To reduce the computational complexity caused by including geometry of the sulci, the model itself was constructed as a 2D planar model containing the lateral ventricle and the sulci as major geometrical features. It also included various features of the exact anatomical geome-

try of the brain; the gray and white matter, the falx cerebri, and the skull are developed as a physical part, whereas the outer layer of the cerebral cortex associated with the capillaries, the ependyma, and the dura mater is represented by the interface at the boundary of the parenchyma (Fig. 1).

## Material Properties

Peña et al.<sup>48</sup> suggested 3 hypotheses regarding the cause of periventricular lucency, namely periventricular stress concentrations,<sup>44</sup> CSF intrusion into the white matter due to the mechanical disruption of the ependymal,<sup>45</sup> and the geometry (concavity of horns) of the wall.<sup>48</sup> There is not much evidence for the disruption of the ependyma, even though the intercellular spaces of the ependymal cells may be overstretched or even torn, so that CSF can easily infiltrate into the periventricular tissue, according to Peña's anatomical FEM simulation. Therefore, the ependymal membrane in the model is considered to be semipermeable.<sup>17</sup>

The falx cerebri and the skull are modeled as linear-elastic materials. The parenchyma is modeled as an isotropic, porohyperelastic material, containing a solid hyperelastic matrix saturated with interstitial fluid; in other words, a porous solid having a nonlinear stress-strain relationship.<sup>7,53</sup> The heterogeneity of the parenchyma is addressed by assigning different properties to gray and white matter, but no additional local variations in mechanical properties of the brain are considered. Brain porosity and perfusion by CSF are implemented using a standard poro-elastic consolidation theory.<sup>7</sup> The material properties used in the model are given in Table 1.<sup>2,16,31,33,42,44,51,52,57,58,61,68</sup>

## Brain Loading and Boundary Conditions

The outer boundary of the tissue is anatomically presumed to be the capillary region, which is located in the cerebral cortex. With the support of Greitz's findings,<sup>22</sup> it is hypothesized that interstitial fluid drains out of the capillaries. The pore pressure is set to 0 along this boundary, implying a permeable boundary that allows the fluid to flow freely across the layer. In addition, this pressure provides a reference for the transmante pressure ( $P_t$ ), which in our model is defined as the difference between the capillary blood pressure and the ventricular fluid pressure.<sup>48</sup>

Because the model is symmetrical, there is no horizontal displacement of the midline. No fluid flux occurs across the midline boundary, which is therefore modeled as impermeable. As a result, no prescribed pressure needs to be defined along this line. Parenchymal tissue is fixed by the falx cerebri, the end of which is firmly attached to the skull, which is itself fully constrained. There are several contact issues in the model, such as the overlapping of the meshes between adjacent entities. Self-contact was needed for the outer layer of the parenchymal tissue. Normal contact also occurs between the outer layer of the parenchymal tissue and the inner layer of the skull. Finally, contact is considered in the region between the falx cerebri and the outer layer of the parenchymal tissue (Fig. 2).

The loading conditions used to model hydrocephalus and IIH were different in accordance with their differing pathophysiological features. To produce the enlarged or small ventricles, transmante pressure was evenly applied

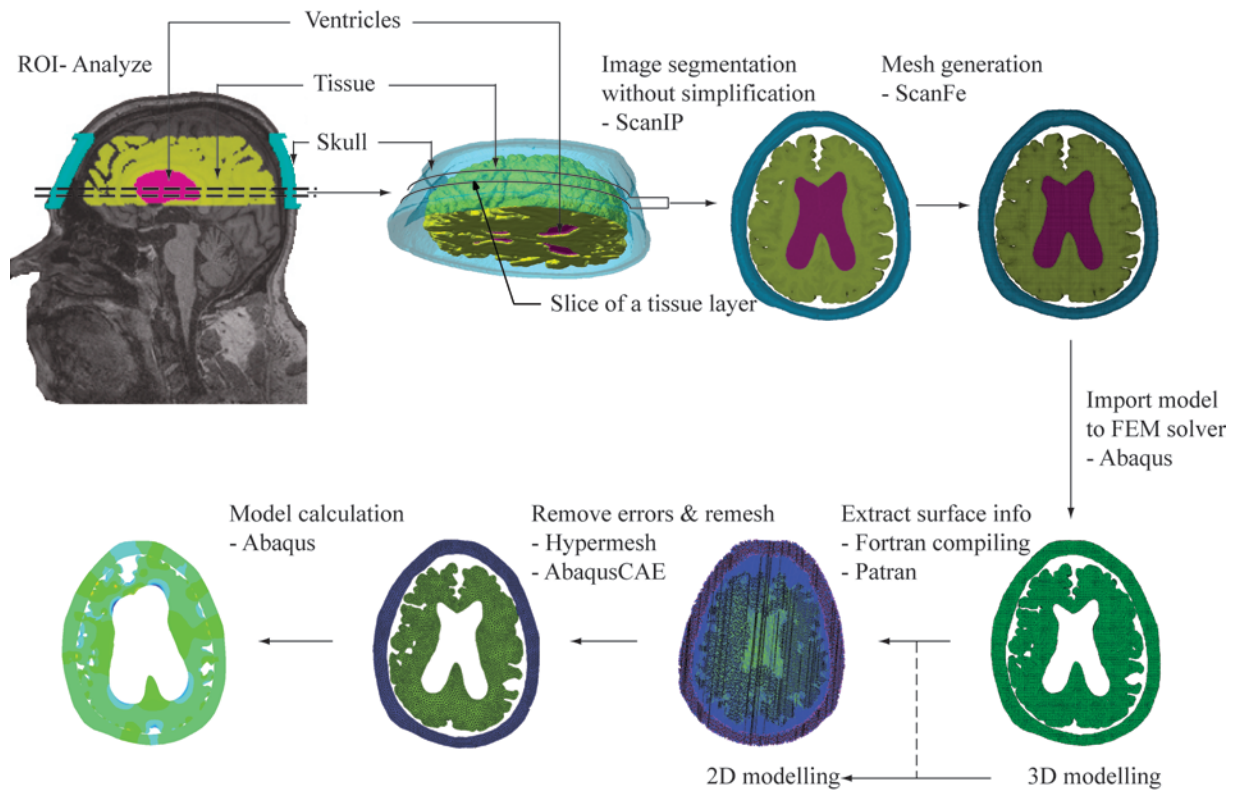


**FIG. 1.** Overview of the model's development. Axial T2-weighted MR images of a healthy human brain were processed using ScanFE to produce a 3D mesh. FORTRAN codes were developed to turn a 3D Abaqus model into a 2D model. Hypermesh (Altair Engineering), a preprocessing software, was used to remove errors and to replace mesh elements. For the detailed process of deriving the model from the MR image, please refer to the *Appendix*. ROI = region of interest.

along the ependyma of the lateral ventricles. For the hydrocephalus model, the transmante pressure at the lateral ventricles was set at an initial value of 0.1 mm Hg. This was gradually increased to 3 mm Hg over a period of 340,000 seconds (4 days), because this time span is considered the minimum period for the development of hydrocephalus.<sup>44</sup> In the IHH model, an initial negative ventricular fluid pressure of -3 mm Hg was applied, this being lower than the capillary pressure ( $P_c$ ), to create an appropriate, negative pressure gradient across the cerebral mantle.

Finally, the results of the simulations were presented as 4 biomechanical parameters, namely the void ratio, the pore pressure, the stress, and the strain. The stress combination at a given point was presented as von Mises stress. The void ratio is defined as the proportion of fluids and solids in an area. The void ratio of a normal brain is known to be 0.2.<sup>44</sup> Thus, a void ratio higher than 0.2 can be interpreted as an increase in fluid content, whereas a 0.2 or lower void ratio indicates a normal state or even a decrease in fluid content. The pore pressure signifies the pressure of fluid filling the pore space; a negative pore pressure indicates the inflow of fluid, whereas 0 or positive pore pressure indicates being free of fluid or an outflow of fluid. Volumetric strain is defined as the change in volume divided by the original volume.<sup>60</sup> When in dilation, the volumetric strain becomes positive, and vice versa. In the case of the 2D model, 2D volumetric strain was applied. The change in the volume on the z axis was assumed to be 0.

## Results

### Simulation of Hydrocephalus

The FEM simulations for hydrocephalus demonstrated the core pathophysiological features of hydrocephalus, namely ventricular expansion and periventricular lucency. Figure 3 left shows the model mesh before and after applying ventricular pressures of 0 and 3 mm Hg.

The parameters of biological importance that were used proved to be good indicators for edema mapping as well as for the detection of ventricular expansion. From the ependymal wall analysis in Fig. 4, it can be seen that there were increases in the magnitude of the void ratio of 0.65 and 0.69 at the frontal and occipital horns, respectively. Similarly, there was an increase in the volumetric strain of 0.32 and 0.34 at the frontal and occipital horns, respectively. Relatively low pore pressures of 0.6 mm Hg and 1 mm Hg were noted at the frontal and occipital horns, whereas the area adjacent to the centrum semiovale showed a much higher magnitude of 2.27 mm Hg in terms of pore pressure. The von Mises stress increased by 0.93 kPa and 0.92 kPa at the frontal and occipital horns, respectively. Thus, edema at the horns of the ventricle is simulated in relation to the features of hydrocephalus.

Ventricular expansion of the wall is demonstrated through an increase in the displacement magnitude. There was a nonuniform displacement along the ependymal wall, with a peak displacement of 19.4 mm in the centrum se-

**TABLE 1. Summary of the material properties of the brain model\***

Property	Value
<b>Parenchyma</b>	
$E_p$ (Pa)	420.5
$\nu_p$	0.35
$C_{10}$ (Pa)	77.9
$D_1$ (Pa <sup>-1</sup> )	$4.28 \times 10^{-3}$
$e$	0.2
$\rho_p$ (kg <sup>-3</sup> ) or (kg/m <sup>3</sup> )	1040
$k$ (m/s)	
White matter	$10^{-7}$
Gray matter	$10^{-9}$
<b>Falx cerebri</b>	
$E_f$ (Pa)	$3.4 \times 10^6$
$\nu_f$	0.45
$\rho_f$ (kg <sup>-3</sup> ) or (kg/m <sup>3</sup> )	1130
$t$ (mm)	2
<b>Skull</b>	
$E_s$ (Pa)	$14 \times 10^9$
$\nu_s$	0.23
$\rho_s$ (kg <sup>-3</sup> ) or (kg/m <sup>3</sup> )	1412

$e$  = void ratio;<sup>47</sup>  $E_f$  = Young's modulus of falx cerebri;<sup>33,59</sup>  $E_p$  = Young's modulus of parenchyma;<sup>17,44</sup>  $E_s$  = Young's modulus of skull;<sup>33,59</sup>  $k$  = permeability;<sup>35</sup>  $t$  = thickness;<sup>70</sup>  $\nu_f$  = Poisson's ratio of falx cerebri;<sup>33,70</sup>  $\nu_p$  = Poisson's ratio of parenchyma;<sup>35,47,51</sup>  $\nu_s$  = Poisson's ratio of skull;<sup>33,70</sup>  $\rho_f$  = density of falx cerebri;<sup>70</sup>  $\rho_p$  = density of parenchyma;  $\rho_s$  = density of skull.<sup>70</sup>

\*  $C_{10}$  and  $D_1$  are calculated from  $E$  and  $\nu$ , and the details of the calculations can be found in the *Appendix*.

miovale area adjacent to the lateral ventricle, whereas the frontal and occipital horns had displacements of 9.4 mm and 12.4 mm, respectively. It was interesting to note an increase in the lengths of ependymal wall and the cerebral cortex outer layer of 28.7 mm and 14.8 mm, from their original lengths of 135 mm and 650 mm, respectively. The contour plots in Fig. 5 represent the parameters of biological importance. Edema mapping is clearly represented in Fig. 5A–E.

**Simulation of IHH**

Both small ventricle formation and cerebral edema presenting as papilledema are simulated by our IHH model. These simulation results have similar clinical features to IHH. Figure 3 right shows the model before and after ventricular pressure reduction from 0 mm Hg to -3 mm Hg.

The same parameters of biological importance successfully indicated cerebral edema-affected areas, as well as the reduction of ventricle size. The results of the ependymal wall analysis reveal an increase in the magnitude of void ratio, volumetric strain, and negative pore pressure in the area adjacent to the centrum semiovale. There were increases in void ratio and volumetric strain of 0.33 and 0.1, respectively, at the area adjacent to the centrum semiovale. A 0 void ratio and negative volumetric strains of -0.66 and -0.49 are predicted at the frontal and occipital horns, respectively. Consequently, except at the frontal

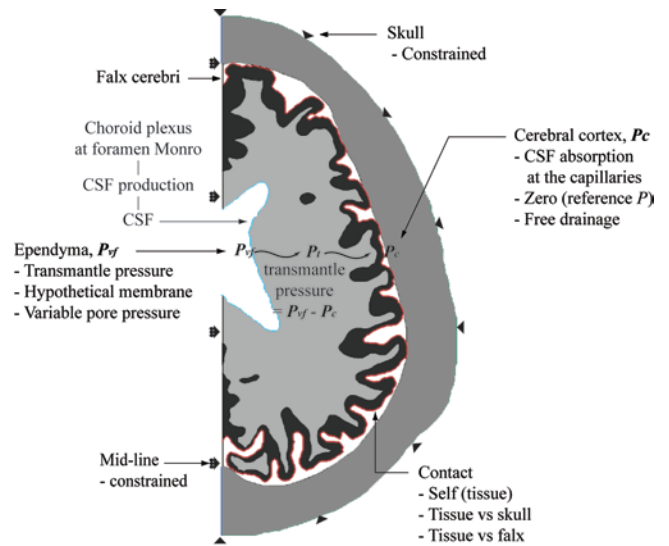


**FIG. 2.** Schematic illustrations of the load and boundary conditions. The load and boundary conditions applied in the FEM, the ventricle and capillaries, have prescribed pressures, the skull is fully constrained, and the midline boundary is constrained against the x-direction displacement. The outer boundary of the parenchyma is assumed to be the capillaries, where the interstitial fluid drains out.

and occipital horns, increased tissue volume is indicated around the ventricle. A negative pore pressure (-0.09 mm Hg) was also noted in the area adjacent to the centrum semiovale. As a result, there is a significant difference in these parameters at the frontal and occipital horns when compared with the area adjacent to the centrum semiovale. This indicates less accumulation of interstitial fluid at the horns compared with the centrum semiovale area.

The maximum void ratio and the volumetric strain recorded at the centrum semiovale reveals edema, and this mapping correlates with the clinical features of IHH. There were also increases in the von Mises stress at the frontal and occipital horns, with 0.57 kPa and 0.34 kPa, respectively. Small ventricle formation is revealed through a maximum inward displacement of 7 mm. We also noted an increase of 5.7 mm in the length of the ventricle ependyma from the original length of 135 mm. However, the outer layer of the cerebral cortex had no significant change in length. Contour plots in Fig. 6 represent the simulation results of cerebral edema mapping as well as a small ventricle and compression of the brain parenchyma. Figure 5F, G, I, and J represent the areas affected by cerebral edema, whereas Fig. 5H shows the areas that are compressed.

A direct comparison between clinical MR images shows that the important features of hydrocephalus and IHH are simulated (Fig. 6). Periventricular lucency, ventricular expansion, small ventricle, cerebral edema, and compression can be directly matched between the FEM simulation and the MR images for hydrocephalus and IHH. In addition, the parameters of biological importance used for edema mapping (void ratio and volumetric strain) both produce reasonably accurate or identical results in comparison with the MR images. For example, in the IHH

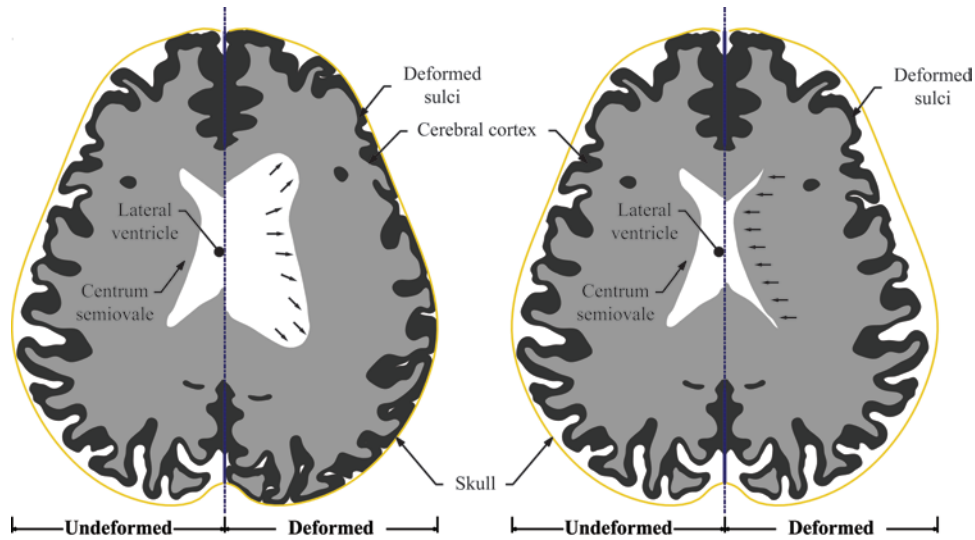


**FIG. 3.** Undeformed versus deformed models of hydrocephalus and IHH. **Left:** Undeformed and deformed hydrocephalus finite model simulation illustrating the ventricular dilation and sulci deformation. **Right:** Undeformed and deformed IHH FEM simulation illustrating small ventricle formation and the expansion of the periventricular tissue.

model, areas of expansion due to edema are directly correlated to the areas of expansion in the MR image, as indicated by the arrows in Fig. 6C and D.

## Discussion

### Technical Implication

In vivo mechanical measurements of brain material are necessarily limited. For this reason, the validation of medical hypotheses of neurological disorders involving brain

deformation is often frustrating. With appropriate material properties and boundary conditions, the FE analysis can be an effective alternative to in vivo measurements. There have been a number of FE analysis studies on hydrocephalic brains in which various models were used. However, even though these linear or nonlinear material models are useful for explaining aspects of hydrocephalic brain distortion, the previous models have neglected either the biphasic nature of the brain (having both solid and

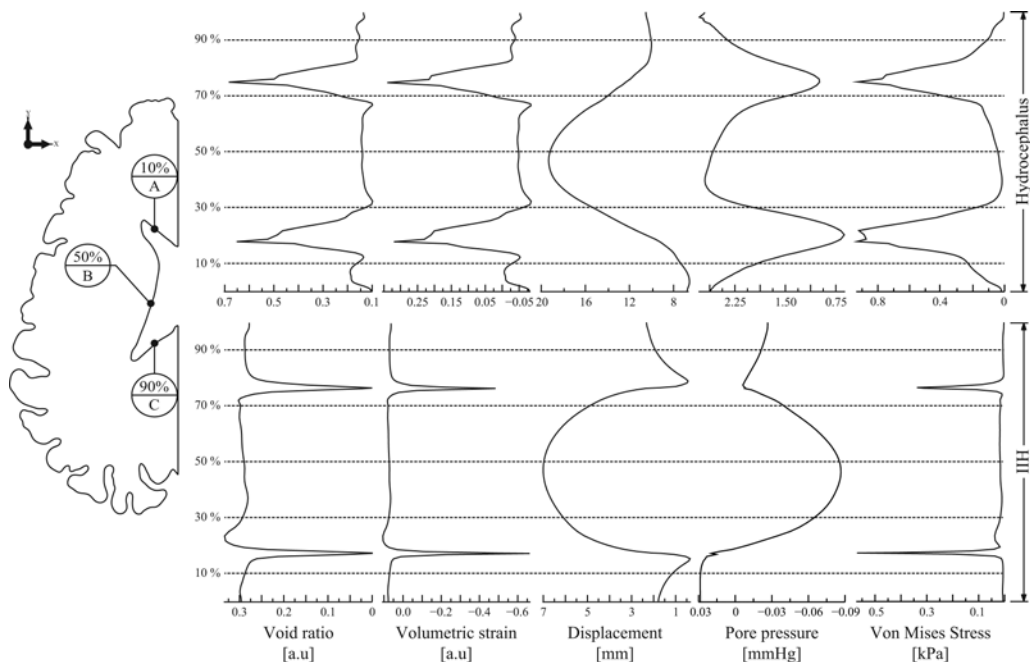


**FIG. 4.** Ependymal wall analysis comparison of the lateral ventricle. The hydrocephalus (upper) and IHH (lower) were simulated by using 5 key parameters, namely void ratio, volumetric strain, displacement (mm), pore pressure (mm Hg), and von Mises stress (kPa). The percentages from 0% to 100% represent the normalized distance along the ependymal wall of the lateral ventricle.

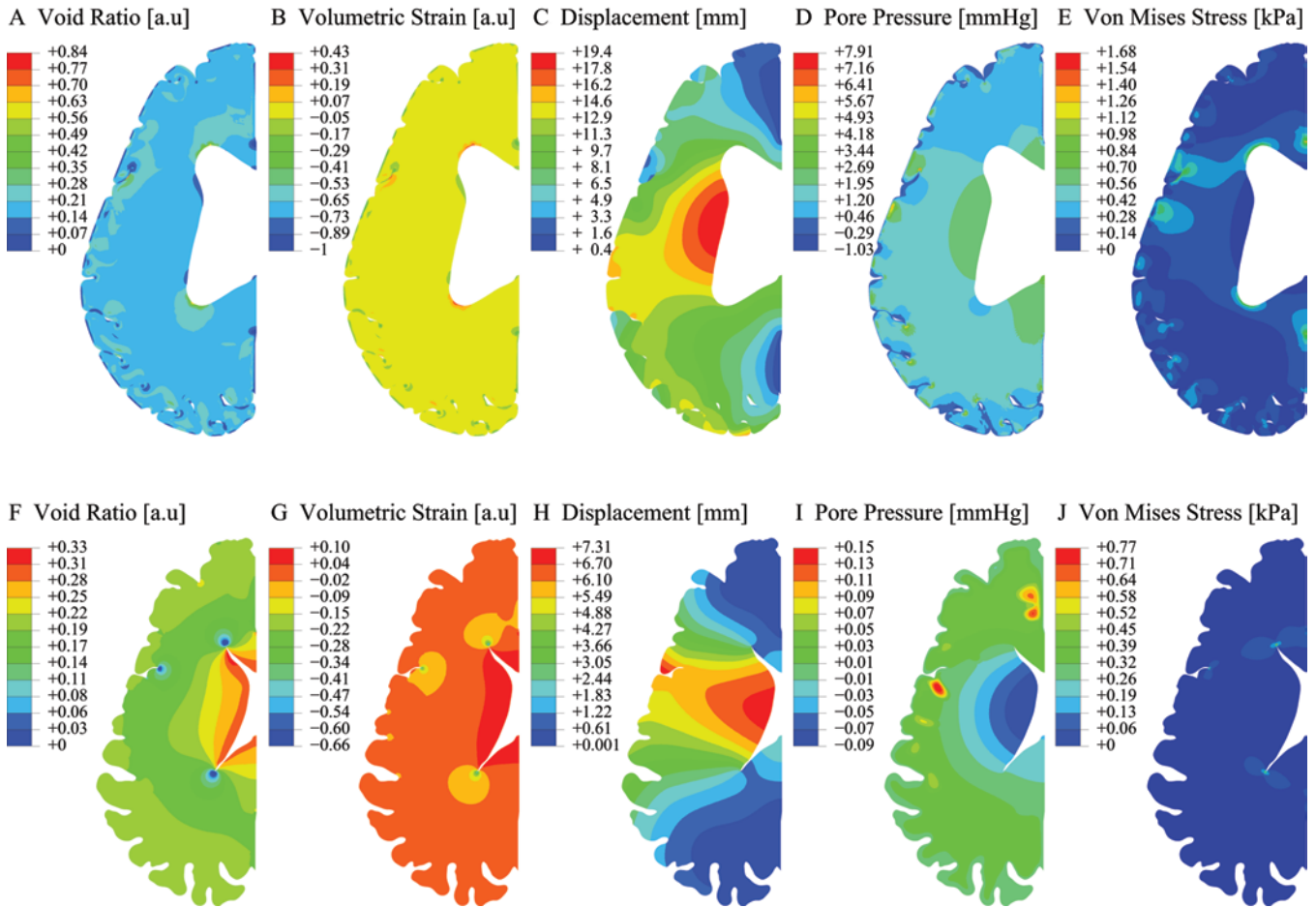


**FIG. 5.** Contour plot representations: the plots of the void ratio, volumetric strain, displacement, pore pressure, and von Mises stress from the FEM simulation results for hydrocephalus (A–E) and IIH (F–J). a.u. = arbitrary units.

fluid phases) in the hyperelastic models, or the nonlinear stress-strain response of the solid phase (the neurons and neuroglia) of brain tissue in the poroelastic models.<sup>20</sup> For the brain material models to reflect the material properties of the brain accurately, both poroelasticity and hyperelasticity must be incorporated.

In the existing literature, the Biot model is widely used to model poroelastic structures, including the solid phase of a porous property fully saturated with a significant quantity of fluid.<sup>7,25,53</sup> With hyperelasticity combined, several recent studies obtained satisfactory results.<sup>21,54,59</sup> Furthermore, the neo-Hookean model is well suited to describing the hyperelastic, nonlinear behavior of compressible biological tissue. The model in this study is based on a recent development of the Biot model.<sup>16</sup> Extensions to the model are implemented by the neo-Hookean model that allows for nonlinear, elastic behavior in the solid structure. The resulting porohyperelastic model is grounded in soil mechanics, because brain tissue is a material that can be characterized by a nonlinear constitutive relationship. This relationship can be then used, together with the laws of continuum mechanics, to predict the deformation response within the material due to imposed stress or displacement at the boundary. To the best of our knowledge, the model

used in this study is the first porohyperelastic model to incorporate complex anatomical geometry, including sulci.

### Representation of the Pathological Features of Hydrocephalus and IIH

The common features of hydrocephalus and IIH are disturbances in normal CSF circulation, which may be corrected by shunt placement.<sup>5,50</sup> These diseases also show intracranial hypertension. However, there are several significant differences between them. In hydrocephalus, the raised ventricular fluid pressure is the main factor contributing to intracranial hypertension via ventriculomegaly. This increased ventricular fluid pressure also exists in IIH, but is compensated for by even higher parenchymal tissue resistance, caused by cerebral edema. Thus, small ventricles are often observed in IIH. In addition, periventricular lucency is an indication of hydrocephalus, whereas diffused brain edema is present in IIH.<sup>14,43,47</sup>

One of the pathological features of periventricular lucency is the accumulation of a fluid, referred to as interstitial edema, at the horns.<sup>46,48,59</sup> For the hydrocephalus model, a positive volumetric strain, which occurs when there is an increase in tissue volume due to fluid accumulation confirming edema, is revealed at the frontal and occipital

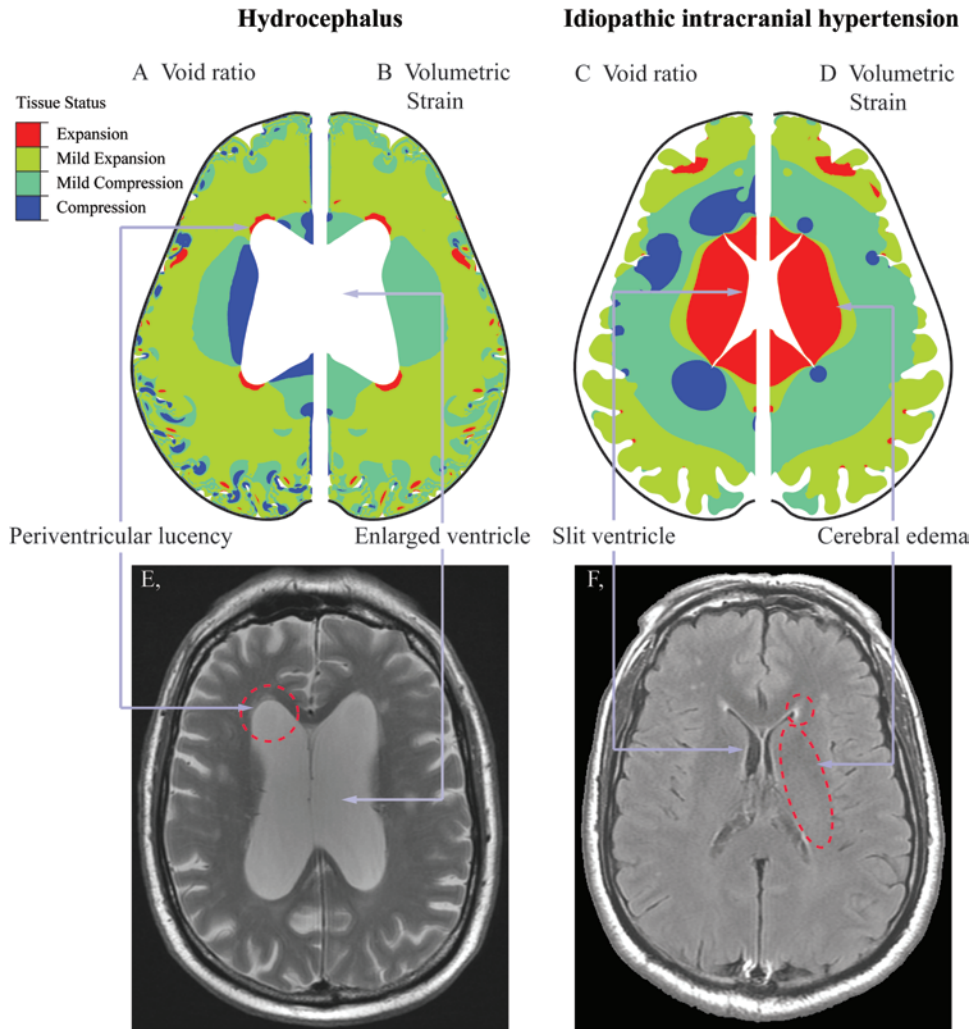


**FIG. 6.** Comparison of FEM simulation results (upper) and clinical MR images (lower). Mild expansion and mild compression are presumed to be equal to 10% of the maximum expansion and compression. Void ratio and volumetric strain similarities as edema mapping indicators are illustrated.

horns. The void ratio can be used as a good indicator for edema,<sup>48</sup> with areas of void expansion relating to fluid accumulation. In the hydrocephalus model, there is an increase of the void ratio to 0.61 and 0.7 at the frontal and occipital horns, respectively. The initial void ratio was set as 0.2.<sup>44</sup> The results of the hydrocephalus model in this study reveal periventricular lucency, providing a physical model for periventricular edema at the frontal and occipital horns. In addition, periventricular edema occurs even though the ependymal membrane is considered to be semipermeable.

For normal conditions in the brain, there is no significant resistance preventing fluid from flowing to the lateral ventricles.<sup>1,14,15</sup> However, in IiH, the transmantle pressure is nearly 0, resulting in slow fluid flow from the capillaries. This might be the reason there is a slow progression in IiH.<sup>1</sup> Figure 5 shows volumetric straining, indicating cerebral edema, with the assumption that the fluid in the tissue is fully saturated, with both solid and fluid elements incompressible. In IiH, the expansion is observed adjacent

to the lateral ventricles. In hydrocephalus, volumetric expansion associated with a tensile stress is shown in red. This red area is presumed to indicate cerebral edema. Furthermore, in IiH, a significant increase in the void ratio is observed around the ventricles, whereas for hydrocephalus, significant expansion occurs at the frontal and occipital horns.

### Hydrocephalus and IiH: Opposite Manifestations of Disturbed CSF Absorption

The proposed model demonstrated key features of brain deformation in hydrocephalus and IiH. More importantly, the model simulated and derived the results with the change in transmantle pressure gradient being the only difference between the 2 neurological disorders. One might expect the results of the present study to be based on false assumptions, because the issue of the transmantle pressure gradient itself is highly controversial. Some studies conclude that the transmantle pressure gradient is very small, if it exists at all.<sup>49,56</sup> However, a recent theoretical study

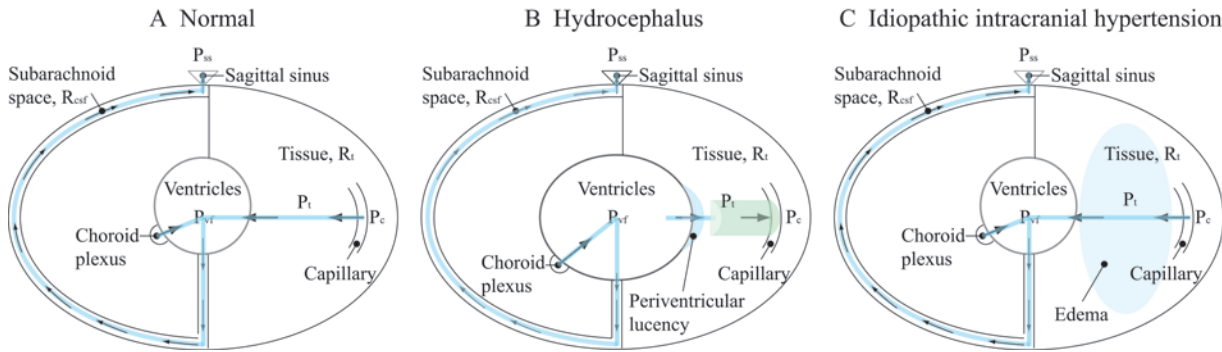


**FIG. 7.** Schematic diagram of the physiology of normal (A), hydrocephalic (B), and idiopathic intracranial hypertensive (C) brains. In hydrocephalus, capillary pressure ( $P_c$ ) is less than ventricular fluid pressure ( $P_{vf}$ ) due to the disturbed CSF absorption, thus resulting in positive transmantle pressure ( $P_t$ ). The increased transmantle pressure forces the interstitial fluid to flow to the capillaries, which allows ventriculomegaly. On the other hand, in IIH, the capillary pressure becomes higher due to venous stenosis, leading to a very small or even negative transmantle pressure gradient level. This enables the accumulation of interstitial fluid in the parenchyma, thus resulting in hypertension, often with small ventricles, although ventricular fluid pressure remains high.  $P_{ss}$  = sagittal sinus pressure;  $R_{csf}$  = regional CSF;  $R_t$  = tissue resistance.

also suggests that CSF-related brain deformation does not require a large pressure gradient.<sup>36</sup> Currently, there is no definite evidence to accept or abandon the concept of transmantle pressure gradient, which is all the more reason to construct a versatile model capable of manipulating the condition in question (Fig. 7).

The brain parenchyma, when fully saturated with interstitial fluid, is incompressible or nearly incompressible. In addition, the intracranial system is encased by an effectively rigid body.<sup>41,48,59</sup> Therefore, enlargement of the ventricles can only occur in situations in which there is volumetric reduction of the parenchyma.<sup>22,23</sup> This raises the question of where the drainage of interstitial fluid occurs. Previous research<sup>24</sup> indicates both the absorption of CSF by brain capillaries, and that CSF is transported via vascular pulsations in the subarachnoid space. In the progression of hydrocephalus, an increase in ventricular pressure due to the disturbance in CSF absorption<sup>12,19</sup> induces a reversal of the pressure gradient across the cerebral mantle. Because of the high ventricular fluid pressure, the interstitial fluid pressure is higher than the capillary pressure in hydrocephalus. Therefore, hypothetically, interstitial fluid can be wrung out of the capillaries,<sup>18,38–40,62</sup> resulting in the volumetric reduction of brain parenchyma known as ventriculomegaly.

On the other hand, the absence of volume reduction of the parenchyma implies that no efflux of the interstitial fluid occurs through either the ventricle or the capillaries.<sup>15</sup> In IIH, high intraventricular pressure as well as high capillary pressure is commonly revealed,<sup>1,50</sup> due to the venous stenosis.<sup>3,8,26,27,30,32</sup> Thus, the transmantle pressure between the 2 compartments (the ventricular space and capillaries) must be quite low or even negative. The low transmantle pressure associated with the resistance of extracellular channels results in difficulty in inducing the interstitial fluid's convective flux; consequently, intratissue water accumulation occurs, leading to an increase of intracranial pressure via water content in the brain.<sup>18,38–40,62</sup> This typically appears in IIH, and is viewed as vasogenic cerebral edema of uncertain origin, affecting the CSF pressure within the sheath of the optic nerve in relation to orbital

venous pressure.<sup>15</sup> Therefore, IIH-affected patients often show a degree of visual loss.<sup>20</sup>

### Capillary Absorption of CSF in IIH and Hydrocephalus

The conventional view of CSF dynamics states that most, if not all, CSF is absorbed at the superior sagittal sinus via arachnoid granulation.<sup>9</sup> Whereas this may explain how hydrocephalus can develop, it does not provide a clear explanation regarding the development of IIH. Meanwhile, the model in this study is based on recent theories and the discovery that a significant amount of CSF is absorbed in the capillary region<sup>22</sup> and will later drain out through the venous sinuses.<sup>3,8,26,27,30,32</sup> With this modified view of CSF dynamics, the reason that impaired CSF absorption manifests as hydrocephalus or IIH can be considered.

Because the ventricular fluid pressure is elevated in both diseases, the differentiating factor would be the capillary pressure, which is heavily affected by venous outflow. In hydrocephalus, the ventricular fluid pressure increases due to the blockage at the arachnoid granulation. The high transmantle pressure gradient causes the efflux of interstitial fluid to the capillary; thus, the brain deforms with ventriculomegaly. On the contrary, in IIH, the capillary pressure becomes elevated due to venous stenosis. This causes a low or even negative transmantle pressure gradient and no efflux of interstitial fluid into the capillary, subsequently inducing the accumulation of interstitial fluid at the brain parenchyma. This then causes intracranial hypertension, due to cerebral edema without ventriculomegaly. In addition, a similar mechanism may lead to slit ventricle syndrome in patients with shunts, as hypothesized and documented in earlier studies.<sup>3,29</sup>

In summary, the FEM used in this study correlates in many aspects with the clinical features of the 2 major neurological disorders associated with CSF-related brain deformation. The results of the model support the concept of the transmantle pressure gradient as a major factor in CSF-related brain deformation. The clinical application of the FE brain model will help to anticipate the pathogenesis of space-occupying lesions in the brain. In reality, various

reasons for inducing fluctuations in transmante pressure gradients should be considered to fully explain the varying degrees of brain deformation. This may help to provide better prognoses for individual patients and could be applicable for a more tailored treatment of patients in the future.

## Conclusions

The proposed 2D FEM of the head has suggested the mechanisms of the development of both hydrocephalus and IHH. Specifically, periventricular lucency and ventricular enlargement correlated with the clinical results for hydrocephalus. Cerebral edema presenting as papilledema in IHH was also demonstrated using the model. Our results seem to support the hypothesis that IHH and hydrocephalus, as CSF absorption-related neurological disorders, are diseases with opposite pathogenesis, and that the reabsorption of interstitial fluid in the capillaries is a key mechanism for the phenomenon.

## Appendix

### Derivation of 2D Model From MR Image

The MR images were processed using ScanIP (Simpleware Software Ltd.) to obtain brain cross-sections that allow the region of interest (i.e., the brain) to be segmented. From these sections, ScanFe (Simpleware Software Ltd.) made it possible to produce a 3D FE mesh of the sliced brain and to export the model in a form compatible with Abaqus.

With the selected work flow of the geometrical model, deriving a 2D model from the 3D FE mesh was not trivial. The MR source images contain voxels that represent thickness, but the desired 2D model has no thickness. Thus, to get the 2D model from the 3D Abaqus input file derived from ScanFE, in-house FORTRAN codes were developed and used. The 2D surface of the extracted model has a relatively poor mesh quality. Hypermesh (Altair Engineering),

a preprocessing software, was used to remove errors, repair mesh elements, build in the surface of the model and, ultimately, to export the model for performing an Abaqus FEM analysis.

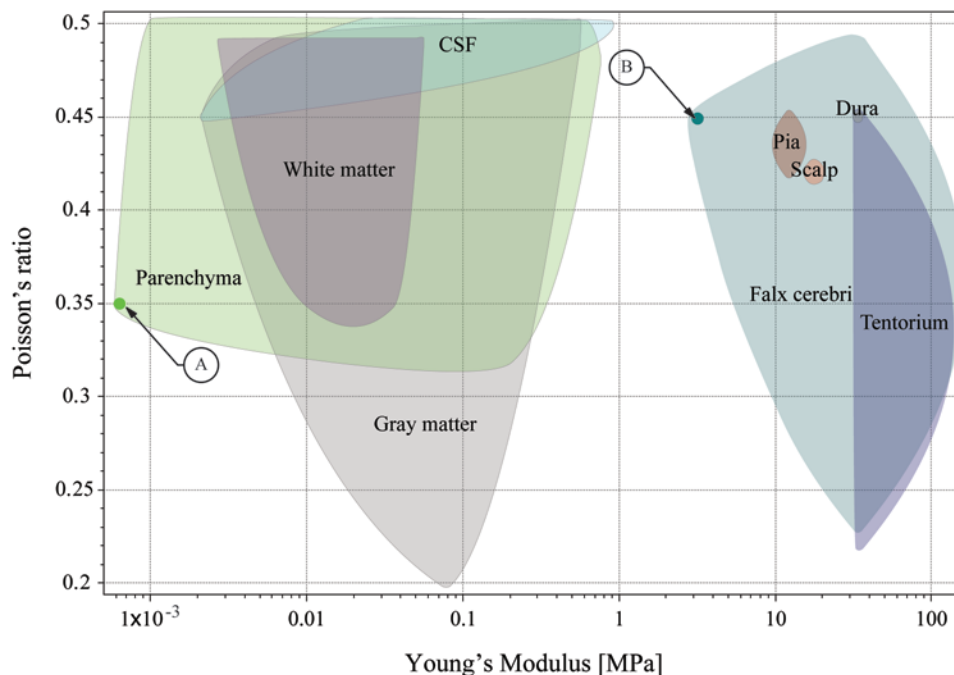
An FE mesh was generated with 4-node quadrilateral elements by using an automated mesh-generating algorithm. For the simulations, a plane strain model is used to represent a slice of the brain and skull. The changes in geometry in the out-of-plane direction are considered to be sufficiently gentle to make such an approximation reasonable. An alternative 2D approach would be to adopt an axisymmetric model, but the geometry, especially around the frontal and occipital horns of lateral ventricle, would no longer be effectively represented.

### The Material Properties and Derivation of Field Equations

The model used reduced-integration Abaqus elements CPE4RP (4-node bilinear displacement and pore pressure, reduced integration with hourglass control), CPS4R (4-node bilinear, reduced integration with hourglass control), CPE4R (4-node bilinear, reduced integration with hourglass control), and CPE3 (3-node, linear) for the parenchymal tissue, the skull, and the falx cerebri. The total number of elements in the model is approximately 18,000. Abaqus 6.12-3 nonlinear element code was used with implicit time integration associated with soil and hyperelastic analysis, accounting for both the constitutive and geometrical nonlinearity.

The major difference between the porohyperelastic model (which this study used) and the previous model comes from the assumption about the material property of the brain parenchyma. The porohyperelastic model describes the brain as a hyperelastic solid matrix, saturated with interstitial fluid.<sup>7,53</sup> The Young modulus of the brain parenchyma was adopted from an existing study.<sup>42</sup> Considering the compressibility of the solid matrix of the parenchyma, Poisson's ratio was set as 0.35.<sup>16,33,44</sup> The material properties of the rest of the compartments of the model (i.e., the falx cerebri and skull) are considered to be linear-elastic materials. Thus, the material properties (Young's modulus, density, and Poisson's ratio) of these compartments came from previous studies<sup>2,31,34,51,52,57,58,61</sup> (Appendix Fig. 1).

The material response is the combination of neo-Hookean hyperelastic and volumetric porous material models, simulated using



**APPENDIX FIG. 1.** Graphic representation of known value of Young's modulus and Poisson's ratio on various intracranial entities. The dots labeled A and B indicate the values used in this study.

Abaqus 6.12. According to the Abaqus user manual,<sup>13</sup> the strain energy potential  $U$  (for the compressible neo-Hookean material model) is of the form

$$U = C_{10}(\bar{I}_1 - 3) + \frac{1}{D_1}(J - 1)^2, \quad (\because J_{el} = \frac{J}{J_{th}}, J_{th} = (1 + e_{th})^3),$$

where  $J_{el}$  is the elastic volume ratio,  $J_{th}$  is the thermal volume ratio,  $e_{th}$  is the linear thermal extension,  $\bar{I}_1$  is the measure of the distortion in the material, and  $C_{10}$  and  $D_1$  are material parameters. The  $C_{10}$  parameter describes the shear behavior of the material, and the  $D_1$  parameter introduces compressibility. The tissue material is compressible; thus  $D_1$  should not be 0. The initial shear modulus,  $\mu_0$ , and bulk modulus,  $K_0$ , are given by  $\mu_0 = 2C_{10}$  and  $K_0 = 2/D_1$ .

Based on the above relationships, we can calculate  $C_{10}$  and  $D_1$  from typical material properties (i.e., Young's modulus and Poisson's ratio).

The porous material model can be expressed in the form of  $\sigma = \mu f(\varepsilon)$  where the function of  $\varepsilon$  is nonlinear and  $\mu$  is a normalizing parameter. The porosity was obtained using Forchheimer's law. This can be written as

$$f = -\frac{k}{\gamma_w} \left( \frac{\partial u_w}{\partial x} - \rho_w g \right),$$

where  $f$  is volumetric flow rate,  $k$  is permeability,  $\gamma_w$  is wetting fluid-specific weight,  $u$  is wetting fluid pore pressure,  $x$  is position,  $\rho_w$  is wetting fluid density, and  $g$  is gravity.

## Acknowledgments

We are grateful to Drs. R. Jena (Department of Oncology) and J. Pickard (Department of Neurosurgery), both from Addenbrooke's Hospital, Cambridge, UK.

## References

- Ball AK, Clarke CE: Idiopathic intracranial hypertension. **Lancet Neurol** 5:433–442, 2006
- Bandak F, Eppinger R: A three-dimensional finite element analysis of the human brain under combined rotational and translational accelerations. Presented at the **38th Stapp Car Crash Conference**, Fort Lauderdale, FL, 1994 (<http://papers.sae.org/942215/>) [Accessed December 18, 2014]
- Bateman GA: Hypertensive slit ventricle syndrome: pseudotumor cerebri with a malfunctioning shunt? **J Neurosurg** 119:1503–1510, 2013
- Bateman GA, Loiselle AM: Can MR measurement of intracranial hydrodynamics and compliance differentiate which patient with idiopathic normal pressure hydrocephalus will improve following shunt insertion? **Acta Neurochir (Wien)** 149:455–462, 2007
- Bateman GA, Smith RL, Siddique SH: Idiopathic hydrocephalus in children and idiopathic intracranial hypertension in adults: two manifestations of the same pathophysiological process? **J Neurosurg** 107 (6 Suppl):439–444, 2007
- Binder DK, Horton JC, Lawton MT, McDermott MW: Idiopathic intracranial hypertension. **Neurosurgery** 54:538–552, 2004
- Biot MA: General theory of three-dimensional consolidation. **J Appl Phys** 12:155–164, 1941
- Bono F, Giliberto C, Mastrandrea C, Cristiano D, Lavano A, Fera F, et al: Transverse sinus stenoses persist after normalization of the CSF pressure in IHH. **Neurology** 65:1090–1093, 2005
- Brodbelt A, Stoodley M: CSF pathways: a review. **Br J Neurosurg** 21:510–520, 2007
- Cheng S, Bilston LE: Computational model of the cerebral ventricles in hydrocephalus. **J Biomech Eng** 132:054501, 2010
- Clatz O, Litrico S, Delingette H, Paquis P, Ayache N: Dynamic model of communicating hydrocephalus for surgery simulation. **IEEE Trans Biomed Eng** 54:755–758, 2007
- Dandy WE: Extirpation of the choroid plexus of the lateral ventricles in communicating hydrocephalus. **Ann Surg** 68:569–579, 1918
- Dassault Systèmes: **Abaqus 6.12 Theory Manual**. Providence, RI: Dassault Systèmes Simulia Corp, 2012 (<http://web.ppf:2080/v6.12/books/stm/default.htm>) [Accessed December 18, 2014]
- Dessardo NS, Dessardo S, Sasso A, Sarunić AV, Dezulović MS: Pediatric idiopathic intracranial hypertension: clinical and demographic features. **Coll Antropol** 34 (Suppl 2):217–221, 2010
- Dhungana S, Sharrack B, Woodroffe N: Idiopathic intracranial hypertension. **Acta Neurol Scand** 121:71–82, 2010
- Dutta-Roy T, Wittek A, Miller K: Biomechanical modelling of normal pressure hydrocephalus. **J Biomech** 41:2263–2271, 2008
- Ebinger M: Core topics in neuroanesthesia and neurointensive care. **Arch Neurol** 69:788–789, 2012
- Fishman RA, Greer M: Experimental obstructive hydrocephalus. Changes in the cerebrum. **Arch Neurol** 8:156–161, 1963
- Fode NC, Laws ER Jr, Sundt TM Jr: Communicating hydrocephalus after subarachnoid hemorrhage: results of shunt procedures. **J Neurosurg Nurs** 11:253–256, 1979
- Friedman DI, Jacobson DM: Diagnostic criteria for idiopathic intracranial hypertension. **Neurology** 59:1492–1495, 2002
- Garcia JJ, Smith JH: A biphasic hyperelastic model for hydrocephalus. **Lat Am Appl Res** 40:295–302, 2010
- Greitz D: Cerebrospinal fluid circulation and associated intracranial dynamics. A radiologic investigation using MR imaging and radionuclide cisternography. **Acta Radiol Suppl** 386:1–23, 1993
- Greitz D: Radiological assessment of hydrocephalus: new theories and implications for therapy. **Neurosurg Rev** 27:145–167, 2004
- Greitz D, Greitz T, Hindmarsh T: A new view on the CSF-circulation with the potential for pharmacological treatment of childhood hydrocephalus. **Acta Paediatr** 86:125–132, 1997
- Hakim S, Venegas JG, Burton JD: The physics of the cranial cavity, hydrocephalus and normal pressure hydrocephalus: mechanical interpretation and mathematical model. **Surg Neurol** 5:187–210, 1976
- Higgins JN, Gillard JH, Owler BK, Harkness K, Pickard JD: MR venography in idiopathic intracranial hypertension: unappreciated and misunderstood. **J Neurol Neurosurg Psychiatry** 75:621–625, 2004
- Higgins JN, Owler BK, Cousins C, Pickard JD: Venous sinus stenting for refractory benign intracranial hypertension. **Lancet** 359:228–230, 2002
- Iencean SM: Idiopathic intracranial hypertension and idiopathic normal pressure hydrocephalus: diseases with opposite pathogenesis? **Med Hypotheses** 61:526–528, 2003
- Jang M, Yoon SH: Hypothesis for intracranial hypertension in slit ventricle syndrome: new concept of capillary absorption laziness in the hydrocephalic patients with long-term shunts. **Med Hypotheses** 81:199–201, 2013
- Janny P, Chazal J, Colnet G, Irthum B, Georget AM: Benign intracranial hypertension and disorders of CSF absorption. **Surg Neurol** 15:168–174, 1981
- Jiroušek O, Jíra J, Jírová J, Micka M: Finite element model of human skull used for head injury criteria assessment, in Gilchrist MD (ed): **IUTAM Symposium on Impact Biomechanics: From Fundamental Insights to Applications**. Dordrecht, The Netherlands: Springer, 2005, pp 459–468
- Johnston I, Hawke S, Halmagyi M, Teo C: The pseudotumor syndrome. Disorders of cerebrospinal fluid circulation caus-

- ing intracranial hypertension without ventriculomegaly. **Arch Neurol** **48**:740–747, 1991
33. Kaczmarek M, Subramaniam RP, Neff SR: The hydromechanics of hydrocephalus: steady-state solutions for cylindrical geometry. **Bull Math Biol** **59**:295–323, 1997
  34. Kupczik K, Dobson CA, Fagan MJ, Crompton RH, Oxnard CE, O'Higgins P: Assessing mechanical function of the zygomatic region in macaques: validation and sensitivity testing of finite element models. **J Anst** **210**:41–53, 2007
  35. Lefever JA, García JJ, Smith JH: A patient-specific, finite element model for noncommunicating hydrocephalus capable of large deformation. **J Biomech** **46**:1447–1453, 2013
  36. Levine DN: Intracranial pressure and ventricular expansion in hydrocephalus: have we been asking the wrong question? **J Neurol Sci** **269**:1–11, 2008
  37. Levine DN: Ventricular size in pseudotumor cerebri and the theory of impaired CSF absorption. **J Neurol Sci** **177**:85–94, 2000
  38. Lux WE Jr, Hochwald GM, Sahar A, Ransohoff J: Periventricular water content. Effect of pressure in experimental chronic hydrocephalus. **Arch Neurol** **23**:475–479, 1970
  39. McLone DG, Bondareff W, Raimondi AJ: Brain edema in the hydrocephalic hy-3 mouse: submicroscopic morphology. **J Neuropathol Exp Neurol** **30**:627–637, 1971
  40. Milhorat TH, Clark RG, Hammock MK: Experimental hydrocephalus. 2. Gross pathological findings in acute and subacute obstructive hydrocephalus in the dog and monkey. **J Neurosurg** **32**:390–399, 1970
  41. Miller K, Chinzei K, Orsengo G, Bednarz P: Mechanical properties of brain tissue in-vivo: experiment and computer simulation. **J Biomech** **33**:1369–1376, 2000
  42. Miller K, Taylor Z, Nowinski WL: Towards computing brain deformations for diagnosis, prognosis and neurosurgical simulation. **J Mech Med Biol** **5**:105–121, 2005
  43. Nadkarni TD, Rekate HL: Treatment of refractory intracranial hypertension in a spina bifida patient by a concurrent ventricular and cisterna magna-to-peritoneal shunt. **Childs Nerv Syst** **21**:579–582, 2005
  44. Nagashima T, Tamaki N, Matsumoto S, Horwitz B, Seguchi Y: Biomechanics of hydrocephalus: a new theoretical model. **Neurosurgery** **21**:898–904, 1987
  45. Naidich TP, Epstein F, Lin JP, Kricheff II, Hochwald GM: Evaluation of pediatric hydrocephalus by computed tomography. **Radiology** **119**:337–345, 1976
  46. O'Hayon BB, Drake JM, Ossip MG, Tuli S, Clarke M: Frontal and occipital horn ratio: a linear estimate of ventricular size for multiple imaging modalities in pediatric hydrocephalus. **Pediatr Neurosurg** **29**:245–249, 1998
  47. Olivero WC, Rekate HL, Chizeck HJ, Ko W, McCormick JM: Relationship between intracranial and sagittal sinus pressure in normal and hydrocephalic dogs. **Pediatr Neurosci** **14**:196–201, 1988
  48. Peña A, Bolton MD, Whitehouse H, Pickard JD: Effects of brain ventricular shape on periventricular biomechanics: a finite-element analysis. **Neurosurgery** **45**:107–118, 1999
  49. Penn RD, Lee MC, Linninger AA, Miesel K, Lu SN, Stylos L: Pressure gradients in the brain in an experimental model of hydrocephalus. **J Neurosurg** **102**:1069–1075, 2005
  50. Rekate HL: Editorial. Hydrocephalus and idiopathic intracranial hypertension. **J Neurosurg** **107** (6 Suppl):435–438, 2007
  51. Ruan JS, Khalil T, King AI: Human head dynamic response to side impact by finite element modeling. **J Biomech Eng** **113**:276–283, 1991
  52. Sarkar S, Majumder S, Roychowdhury A: Response of human head under static and dynamic load using finite element method. **Trends Biomater Artif Organs** **17**:130–134, 2004
  53. Simon BR: Multiphase poroelastic finite element models for soft tissue structure. **Appl Mech Rev** **45**:191–218, 1992
  54. Smith JH, García JJ: A nonlinear biphasic hyperelastic model for acute hydrocephalus. Presented at the **ASME 2008 Summer Bioengineering Conference**, Marco Island, Florida, June 25–29, 2008 (Abstract) (<http://proceedings.asmedigitalcollection.asme.org/proceeding.aspx?articleid=1849697>) [Accessed December 18, 2014]
  55. Sobeý I, Wirth B: Effect of non-linear permeability in a spherically symmetric model of hydrocephalus. **Math Med Biol** **23**:339–361, 2006
  56. Stephensen H, Tisell M, Wikkelsö C: There is no transmantle pressure gradient in communicating or noncommunicating hydrocephalus. **Neurosurgery** **50**:763–773, 2002
  57. Takhounts EG, Eppinger RH, Campbell JQ, Tannous RE, Power ED, Shook LS: On the development of the SIMon finite element head model. **Stapp Car Crash J** **47**:107–133, 2003
  58. Takhounts EG, Ridella SA, Hasija V, Tannous RE, Campbell JQ, Malone D, et al: Investigation of traumatic brain injuries using the next generation of simulated injury monitor (SIMon) finite element head model. **Stapp Car Crash J** **52**:1–31, 2008
  59. Taylor Z, Miller K: Reassessment of brain elasticity for analysis of biomechanisms of hydrocephalus. **J Biomech** **37**:1263–1269, 2004
  60. Wang H (ed): **Theory of Linear Poroelasticity with Applications to Geomechanics and Hydrogeology**. Princeton: Princeton University Press, 2000
  61. Watanabe D, Yuge K, Nishimoto T, Murakami S, Takao H: Impact injury analysis of the human head. **Autotechnology** **7**:34–37, 2007
  62. Weller RO, Wiśniewski H: Histological and ultrastructural changes with experimental hydrocephalus in adult rabbits. **Brain** **92**:819–828, 1969
  63. Wilkie KP, Drapaca CS, Sivaloganathan S: Aging impact on brain biomechanics with applications to hydrocephalus. **Math Med Biol** **29**:145–161, 2012
  64. Wilkie KP, Drapaca CS, Sivaloganathan S: A theoretical study of the effect of intraventricular pulsations on the pathogenesis of hydrocephalus. **Appl Math Comput** **215**:3181–3191, 2010
  65. Winston KR, Breeze RE: Hydraulic regulation of brain parenchymal volume. **Neurol Res** **13**:237–247, 1991
  66. Wirth B, Sobeý I: An axisymmetric and fully 3D poroelastic model for the evolution of hydrocephalus. **Math Med Biol** **23**:363–388, 2006
  67. Wu JZ, Herzog W, Epstein M: Evaluation of the finite element software ABAQUS for biomechanical modelling of biphasic tissues. **J Biomech** **31**:165–169, 1998
  68. Yoganandan N, Pintar FA, Larson SJ, Sances A Jr (eds): **Frontiers in Head & Neck Trauma: Clinical & Biomechanical**. Amsterdam: IOS Press, 1998
  69. Zienkiewicz OC, Taylor RL (eds): **The Finite Element Method**, ed 4. New York: McGraw-Hill, 1989

---

### Author Contributions

Conception and design: DJ Kim. Acquisition of data: DJ Kim. Analysis and interpretation of data: DJ Kim, H Kim, Park, Hawi. Drafting the article: DJ Kim, H Kim. Critically revising the article: DJ Kim, Sutcliffe. Reviewed submitted version of manuscript: DJ Kim, Min, BJ Kim, Z Czosnyka, M Czosnyka. Approved the final version of the manuscript on behalf of all authors: DJ Kim. Administrative/technical/material support: DJ Kim. Study supervision: DJ Kim.

### Correspondence

Dong-Joo Kim, Department of Brain and Cognitive Engineering, Korea University, Anam-dong, Seongbu-gu, Seoul 136-713, South Korea. email: dongjookim@korea.ac.kr.